INTERNATIONAL JOURNAL FOR NUMERICAL METHODS IN FLUIDS
Int. J. Numer. Meth. Fluids 2004; **46**:793–813
Published online 27 September 2004 in Wiley InterScience (www.interscience.wiley.com). DOI: 10.1002/fld.774

Experimental and numerical analysis of solitary waves generated by bed and boundary movements

L. Cea[1,*,†], A. Ferreiro[2], M. E. Vázquez-Cendón[2] and J. Puertas[1]

[1]*Civil Engineering School, Universidade de A Coruña, Campus de Elviña s/n. CP15192 A Coruña, Spain*
[2]*Faculty of Mathematics, Universidade de Santiago de Compostela, Spain*

SUMMARY

This paper is an experimental and numerical study about propagation and reflection of waves originated by natural hazards such as sea bottom movements, hill slope sliding and avalanches. One-dimensional flume experiments were conducted to study the characteristics of such waves. The results of the experimental study can be used by other researchers to verify their numerical models. A finite volume numerical model, which solves the shallow water equations, was also verified using our own experimental results.

In order to deal with reflection on sloping surfaces and overtopping walls, a new condition for the treatment of the coastline is suggested. The numerical simulation of wave generation is also studied considering the bed movement. A boundary condition is proposed for this case. Those situations when the shallow water equations are valid to simulate this type of phenomena have been studied, as well as their limitations. Copyright © 2004 John Wiley & Sons, Ltd.

KEY WORDS: shallow waters; finite volumes; solitary waves; wet–dry fronts; bed movement

1. INTRODUCTION

Natural hazards, such as tsunamis, avalanches or hill slope sliding in reservoirs have been studied with great interest in the last years. Wiegel [1] was one of the first to carry out laboratory studies of gravity waves generated by the movement of submerged bodies. He made one-dimensional studies in a rectilinear flume and studied the properties of the waves generated (period, maximum wave height, transmission of energy), relating them with the characteristics of the generation movement (shape and dimensions of the submerged body, velocity, acceleration). Wave generation was achieved by sliding a submerged body on a sloping surface. Different properties of the submerged body and different slopes produce different waves. These kinds of experiments have been carried out by several researchers since [2].

In the last years a great number of numerical studies have been made in order to simulate the propagation and runup of long waves (tsunamis) to the coastline. Usually the shallow water

*Correspondence to: L. Cea, Civil Engineering School, Universidade de A Coruña, Campus de Elviña s/n, CP15192 A Coruña, Spain.
†E-mail: ceagomez@usc.es

Received 7 September 2002
Revised 30 April 2004

equations with an adequate treatment of the coastline, where a dry–wet transition occurs, are used to perform these simulations. Experimental laboratory data are used to validate these numerical models.

Tsunamis are long waves, so shallow water models are often used to perform numerical simulations. In these models some simplifications of the real phenomena are assumed. Tests these simplifications are no longer valid. No consideration of the vertical dimension is a simplification that reduces the complexity of the problem and allows for much faster simulations. Lin *et al.* [3] simulate the runup of a breaking solitary wave in a slanted surface, making use of a vertical two-dimensional model as well as a one-dimensional model based on the shallow water equations. They observed some differences in the breaking of the wave, where the shallow water model was more reflective. It is very important to decide which kind of numerical model is needed in each particular case and which are the limitations of each model.

In this paper experimental and numerical studies were performed, and the properties of the waves generated were analysed, trying to assert the limitations of the shallow water equations in the study of this kind of phenomena.

2. NUMERICAL FORMULATION AND DISCRETIZATION

2.1. Shallow water equations

The 1D shallow water equations or Saint-Venant equations are derived after a vertical average of the Reynolds equations for incompressible flow. While obtaining these equations some simplifications are needed. Because of these simplifications, the shallow water equations can be used only if the vertical velocities and accelerations are negligible and if the bed slope is small.

The one-dimensional shallow water equations can be written in conservative form as

$$\frac{\partial h}{\partial t} + \frac{\partial q}{\partial x} = 0 \tag{1}$$

$$\frac{\partial q}{\partial t} + \frac{\partial}{\partial x}\left(\frac{q^2}{h} + \frac{1}{2}gh^2\right) = -gh\frac{\partial z}{\partial x} - gh\frac{n^2 u|u|}{R_h^{4/3}} + \frac{\partial}{\partial x}\left(v_t \frac{\partial q}{\partial x}\right) \tag{2}$$

where $h(x,t)$ is the water depth, $q(x,t) = h(x,t)u(x,t)$ is the mass flow per width unit, $u(x,t)$ is the average horizontal velocity, g is the gravity constant, n is the Manning coefficient, R_h is the hydraulic radius, which is defined as the ratio between the flow area and the wet perimeter, and v_t is the eddy viscosity.

Equations (1) and (2) can be written in vectorial form as

$$\frac{\partial w}{\partial t}(x,t) + \frac{\partial F}{\partial x}(w(x,t)) = \sum_{k=1}^{3} G_k(x, w(x,t)) \tag{3}$$

$$w = \begin{pmatrix} h \\ q \end{pmatrix} \quad F = \begin{pmatrix} q \\ \dfrac{q^2}{h} + \dfrac{1}{2}gh^2 \end{pmatrix} \tag{4}$$

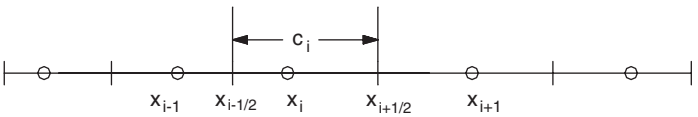

Figure 1. Spatial discretization.

$$G_1 = \begin{pmatrix} 0 \\ -gh\dfrac{\partial z}{\partial x} \end{pmatrix} \quad G_2 = \begin{pmatrix} 0 \\ -gh\dfrac{n^2 u|u|}{R_h^{4/3}} \end{pmatrix} \quad G_3 = \begin{pmatrix} 0 \\ \dfrac{\partial}{\partial x}\left(v_t \dfrac{\partial q}{\partial x}\right) \end{pmatrix} \tag{5}$$

In the turbulent source term G_3 has taken the spatial variation of the eddy viscosity along the calculation domain into account (see Figure 1).

2.2. Numerical discretization

The finite volume method with upwind discretization in space together with an explicit Euler time discretization, is used to solve the system of Equation (3). After the time discretization we obtain

$$\frac{W_{(x)}^{n+1} - W_{(x)}^{n}}{\Delta t} + \frac{\partial F}{\partial x}(W_{(x)}^{n}) = \sum_{k=1}^{3} G_k(x, W^n) \tag{6}$$

where W^n is the value of the conservative variables at time t^n, and W^{n+1} is the value of the variables at time t^{n+1}. The rapid changes in the water-free surface, occurring when generating the solitary waves, make it necessary to use very small time steps in the computations. This time step usually fulfils the CFL condition and thus, an explicit time discretization was chosen. Further details on stability conditions and accuracy are detailed by Vázquez-Cendón in Reference [5].

The spatial domain is discretized by dividing the domain into M nodes X_i $i = 1, M$. The points $X_{i+1/2}$ are defined as the mid points between nodes X_i and X_{i+1}. A cell C_i defined by the points $X_{i-1/2}$ and $X_{i+1/2}$ is assigned to each node X_i.

In this way M cells of variable size are obtained. The length of each cell C_i is $(X_{i+1} - X_{i-1})/2$. The approximate solution W^n is considered as a piecewise constant function. W_i is the mean value of w into the cell C_i.

$$W_{(x)}^{n} = W_i^n \quad x \in C_i \tag{7}$$

After the integration of the expression (6) over the cell C_i we obtain

$$\frac{W_i^{n+1} - W_i^n}{\Delta t} + \frac{F_{i+1/2}^n - F_{i-1/2}^n}{\Delta x_i} = \sum_{k=1}^{3} G_{ki}^n \tag{8}$$

where $F_{i\pm1/2}^n$ is an approximation to the real flow defined by (4) in the cell boundary $X_{i\pm1/2}^n$, and G_{ki}^n is the mean value of the source term G_k in the cell C_i. To calculate this approximation of the real flow in the boundaries of the cell C_i the numerical flux ϕ is used. This numerical flux is given by the Q-scheme of van Leer [4] as

$$\phi(V, W) = \frac{F(V) + F(W)}{2} - \frac{1}{2}|Q(V, W)|(W - V) \tag{9}$$

The matrix Q is the Jacobian of the flow evaluated in the mid point between V and W.

$$Q(V,W)=\frac{\partial F}{\partial W}\left(\frac{V+W}{2}\right) \tag{10}$$

Once the numerical flux has been evaluated, the flow $F^n_{i\pm1/2}$ in (14) can be calculated as

$$F^n_{i+1/2}=\phi(W^n_i,W^n_{i+1}) \tag{11}$$

The variable vector at time t^{n+1}, W^{n+1}, is calculated as

$$W^{n+1}_i=W^n_i-\frac{\Delta t}{\Delta x_i}(F^n_{i+1/2}-F^n_{i-1/2})+\sum_{k=1}^{3}G^n_{ki} \tag{12}$$

The ideas given by Vázquez-Cendón [5] are used to evaluate the discretized source terms G_{ki}. Vázquez-Cendón has shown the convenience of using an upwind discretization of the bed slope source term, developing a scheme to upwind this term in non-structured grids. A study about the convenience of upwinding all the source terms has been made. In this paper, all the source terms will be upwinded with the following expression.

$$G^n_i=\frac{1}{A_i}[A_L\psi_L(x_{i-1},x_i,W^n_{i-1},W^n_i)+A_R\cdot\psi_R(x_i,x_{i+1},W^n_i,W^n_{i+1})] \tag{13}$$

where A_i is the area of the cell $C_i=(x_{i-1/2},x_{i+1/2})$, A_L is the area of the sub cell $C_{iL}=(x_{i-1/2},x_i)$ and A_R is the area of the sub cell $C_{iR}=(x_i,x_{i+1/2})$. The source functions ψ are calculated as

$$\psi_L(x,y,V,W)=[I+|Q(V,W)|Q^{-1}(V,W)]G_k\left(\frac{x+y}{2},\frac{V+W}{2}\right) \tag{14}$$

$$\psi_R(x,y,V,W)=[I-|Q(V,W)|Q^{-1}(V,W)]G_k\left(\frac{x+y}{2},\frac{V+W}{2}\right) \tag{15}$$

In the wave generation areas and in the wet drying fronts, we have to use special boundary conditions which are detailed in the next section.

2.3. Runup of solitary waves: wet–dry condition

When simulating the runup of a solitary wave in sloping surface, there are some cells of the calculation domain which are dry, the water depth in those cells being zero. There is a wet–dry front which must be treated in an adequate manner to avoid introducing errors and non-physical movements in the numerical solution. If the numerical scheme proposed in Section 2.2 is applied to domains with wet–dry fronts, non-physical movements appear in the boundaries, even in a still water stationary situation. As detailed by Brufau [6], these movements are due to the difference between the depth and the bottom gradients in the wet–dry front.

To understand better where the problem is and what the numerical method computes, let us consider a bottom with the following step: $z(x)=z_l$ at the left side and $z(x)=z_r$ at the right side (see Figure 2). At the left side of the step, cells are wet ($h^n=h_l>0$) while at the

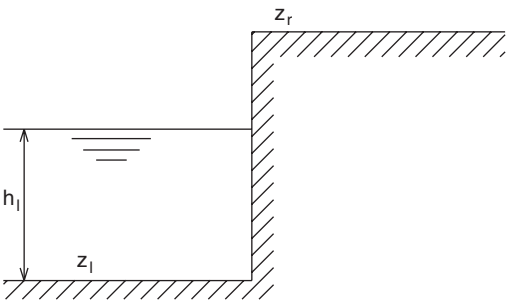

Figure 2. Bottom step.

right side cells are dry ($h^n = h_r = 0$). Let us also suppose that at time step t^n the height of the step is larger than the water-free surface at the left:

$$s_l = z_l + h_l < s_r = z_r + 0 \tag{16}$$

If we apply the numerical scheme previously proposed, the new conservative variables at time t^{n+1} due to the source and flux terms are

$$W_r^{n+1} = \frac{\Delta t}{\Delta x} \begin{pmatrix} \frac{1}{2} q_l + \frac{1}{2} h_l \sqrt{\frac{1}{2} g h_l} \\ \frac{1}{2} \frac{q_l^2}{h_l} + \frac{1}{4} g h_l^2 + \frac{1}{2} q_l \sqrt{\frac{1}{2} g h_l} \end{pmatrix} + \frac{\Delta t}{2\Delta x} \begin{pmatrix} -\sqrt{\frac{1}{2} g h_l} \Delta z \\ -\frac{1}{2} g h_l \Delta z \end{pmatrix} \tag{17}$$

As it can be seen, from a still water initial stationary situation, a cell which was dry at time step t^n is wet at time step t^{n+1}. The water is able to climb a step regardless of its height. To avoid this, a reflection condition in the step is needed. The flow in the wet cell is forced to zero while the water elevation is under the dry cell node.

In addition to using this condition, it is necessary to redefine the bottom as it is detailed by Brufau [6]:

$$\Delta z_m = \Delta h = 0 - h_l \tag{18}$$

With both these conditions, good results are achieved in a stationary situation as well as in a reflection situation. Figure 3 shows an example of the performance of the wet–dry condition.

When simulating the runup of a solitary wave in a sloping surface both conditions are used. Runup in a vertical wall can be simulated with a normal reflection boundary condition if the wall is a non-overtopping wall, but if it is an overtopping wall the wet–dry condition must be used.

2.4. Wave generation

The experiments were carried out in a 15 m long by 60 cm wide flume. The waves are generated by the movement of a slanted paddle. Three different slopes of the paddle were used: 45, 60 and 90°. In all the tests the paddle performs a forward movement at constant velocity and stops without going back to its initial position. The wave generated is expected to

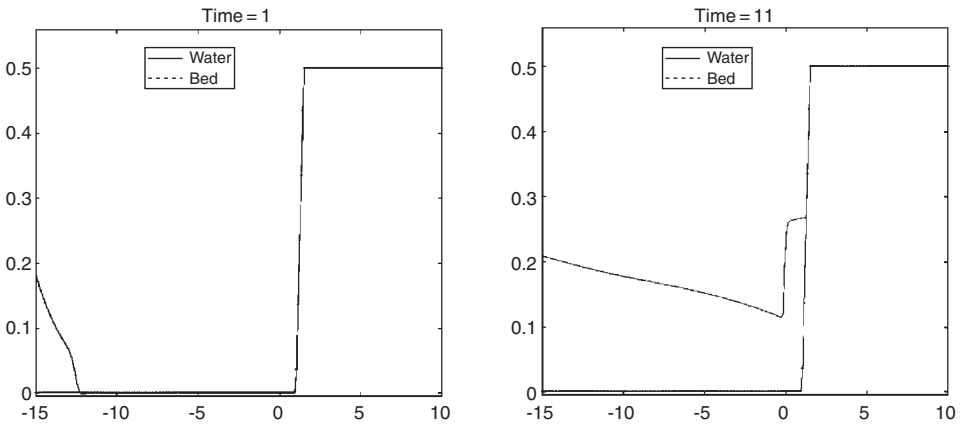

Figure 3. Wet–Dry condition.

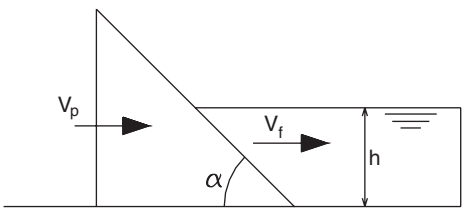

Figure 4. Wave generation by the paddle movement.

have similar features as the waves generated by ground movements, avalanches or tsunamis, so it is possible to verify the performance of the shallow water equations.

Two different processes occur when generating a wave by a paddle movement: the friction between the paddle and the water, and the force perpendicular to the paddle (see Figure 4). The friction between the paddle and the water produces tangential stresses in the bottom of the channel in the same direction as the bed slope. The bigger the paddle rugosity and the relative velocity between the paddle and the water, the bigger are the stresses. The smaller the water depth and the slant of the wave-generation paddle, the more important are the tangential stresses. Considering that in the shallow water formulation the vertical acceleration is negligible, only the horizontal projection of the tangential stresses will be taken into account in the numerical simulation. The second process, and also the most important, is the force applied to the water perpendicular to the paddle slope. In a wave-generation test both processes occur, but their importance is different for each specific test. If the paddle slope is 0° (horizontal), only the water-paddle friction occurs, while if the paddle slope is 90° (vertical), force perpendicular to the paddle is the only process that occurs in the generation of the wave. The expression of the bottom friction source term in the shallow water equations has the following expression:

$$gh\,\frac{n^2[(V_p - V_f)\cos\,\alpha]^2}{h^{4/3}}\,\cos\,\alpha \tag{19}$$

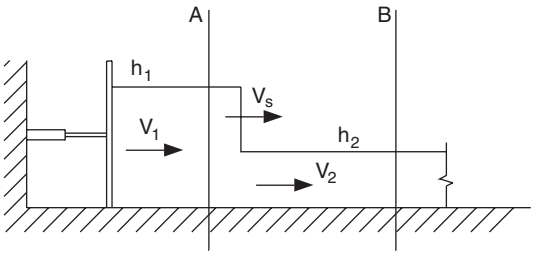

Figure 5. Wave generation by the movement of a vertical wall.

where α is the wave-generation paddle slope, V_p its velocity, V_f the water flow velocity, n the Manning coefficient and h the water depth. This term is equivalent to a bed slope with the following expression:

$$\frac{n^2[(V_p - V_f)\cos\alpha]^2}{h^{4/3}}\cos\alpha \tag{20}$$

In order to know the relative importance of this term, its approximate value in the experiments has been evaluated. The flume Manning coefficient has been approximated to 0.015, the paddle maximum velocity is 0.58 m/s, the minimum paddle slope is 45°, and the minimum water depth is 0.15 m. With these values we obtain the biggest value of the bottom friction term, which is equivalent to a bed slope of 1.79e-4 (0.01°). This value is negligible in the wave generation process, so it will not be considered in the numerical simulation of the essays.

It is necessary to use different numerical schemes to simulate the wave generation depending on the paddle slope. With 45 and 60°, the wave is generated by a bed movement, and it is not necessary to use any special boundary condition. However, when simulating the wave generation by a vertical paddle (90°), this technique produces instabilities and numerical oscillations due to the big bed slope, so it is no longer valid. Numerical instabilities due to the bed slope also appear with the 60° slope, being necessary to use a 2 cm grid in contrast to the 4 cm grid used with the 45° slope. With bigger bed slopes, more refined grids are necessary. With the vertical paddle there is always a point where a discontinuity in the bed occurs, so we have to use a moving boundary condition. In this paper a non-overtopping moving boundary condition has been implemented.

The wave generation by a horizontal movement of a vertical wall is physically equivalent to force a horizontal flux (see Figure 5). With the implemented moving boundary condition, the boundary moves with the paddle, so as the generation process occurs, different cells are implied in the process. Meanwhile, the paddle moves inside the cell C_i, the flux imposed at the boundary $X_{i+1/2}$ is computed as

$$q_{\text{cont}}^{n+1} = \frac{X_w^{n+1} - X_w^n}{t^{n+1} - t^n} h_A \tag{21}$$

The value h_A is equal to the water depth h_i in the time step when the paddle gets into the cell C_i. h_A is constant while the paddle is inside the cell C_i. When the paddle moves into the next cell (C_{i+1}), the new value h_A is taken equal to h_{i+1} in that time step. With this scheme,

the water volume introduced in the domain while the paddle is moving inside the cell C_i is equal to the volume of water in this cell when the paddle gets into it. With this scheme the conservation of mass is achieved.

The water depth h_A at the boundary is considered to be equal to the water depth in the first cell of the calculation domain (C_{i+1}) in the last time step.

$$h_{\text{cont}}^{n+1} = h_{i+1}^{n} \tag{22}$$

This formulation is valid only when simulating non-overtopping moving boundaries. A formulation able to simulate waves generated by the movement of overtopping vertical walls inside the calculation domain is being developed at the moment.

An approximation of the wave generated by the movement of a vertical wall with constant velocity will be obtained below, considering the mass and momentum conservation.

The water velocity at the left of the front is equal to the paddle velocity V_1, h_1 is the water depth at the left of the front; V_2 and h_2 are the velocity and the water depth at the right of the front. The front moves with velocity V_S. Considering the mass and momentum conservation equations between sections A and B, we obtain the expressions (23)–(24)

$$h_1 V_1 - h_2 V_2 = (h_1 - h_2) V_S \tag{23}$$

$$\frac{1}{2} g h_1^2 + h_1 V_1^2 - \frac{1}{2} g h_2^2 - h_2 V_2^2 = (h_1 V_1 - h_2 V_2) V_S \tag{24}$$

The values V_1, V_2 and h_2, are known, so the unknown variables are the front propagation velocity V_S and the water depth at the left h_1. In the laboratory experiments made in this project, V_1 is the paddle velocity, V_2 is zero (the water is still before the experiment starts), and h_2 is the still water depth.

This approximation is only valid when the paddle movement is large enough. When the movement starts, the water level oscillates around h_1, evaluated with the expressions (23) and (24). In Section 4.2 the experimental water depth is compared with the value given by (23) and (24), and some experimental results where these oscillations occur are shown.

3. EXPERIMENTAL PROCEDURE

The experimental tests were carried out in a 60-cm-wide by 15-m-long flume at the CITEEC's hydraulics laboratory (Civil Engineering Technological Innovation Centre). The waves are generated by the horizontal movement of a paddle which is situated at the beginning of the channel. The paddle displacement range is 59.0 cm, and the maximum velocity is 59.0 cm/s. The water depth is measured by conductivity-based depth probes DHI Wave Gauge Type 202 (see Figure 6). The electric signal is received, processed and amplified by a conditioning module of signal DHI Wave Meter Conditioning Module Type 102E. The data acquisition frequency of each wave gauge is set to 100 data per second. All gauges were calibrated before each experimental series. The measurement error of the gauges is 0.7%.

In order to verify the uncertainty in the measurements of the free surface elevation, every test was made twice and no significant differences were observed in the experimental results. In all cases, the differences between the free surface elevation in two different experiments was smaller than 1%.

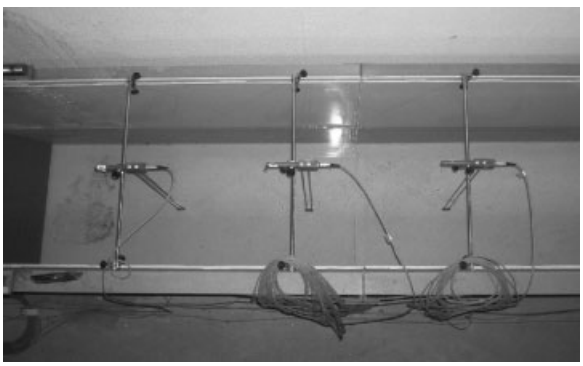

Figure 6. Conductivity-based depth probes.

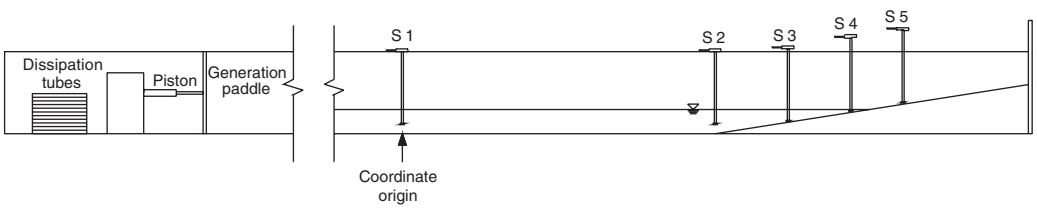

Figure 7. Runup of a solitary wave in a slanted surface (16%).

Table I. Wave gauges position.

S1	S2	S3	S4	S5
0	3.00	3.70	4.30	4.80

Two different series of tests were made. The first series is to analyse the runup of a solitary wave in a slanted surface. A wave is generated and propagated along the flume until it reaches a slanted surface with a 16% slope. In this series of tests five wave gauges are used. First gauge data are used as a boundary condition, and the other four gauges data are compared with numerical results. The tests were performed with four different water depths: 15, 20, 25 and 40 cm. Figure 7 shows the experimental configuration for this series of tests.

Wave gauge positions are shown in Table I. The coordinates are in meters and referenced to the gauge S1.

The second series of tests is to analyse wave generation as well as runup and reflection of waves on a vertical overtopping wall. To accomplish this goal, a wave is generated by the horizontal movement of a slanted paddle. The wave propagates until it reaches a vertical wall 36 cm height by 51 cm long. The tests are conducted with four different water depths: 15, 20, 25 and 30 cm. Depending on the water depth, on the paddle slope and on the paddle movement, the wall may be overtopped or not by the wave. Measurements are registered in five points. Figure 8 shows the configuration of these tests.

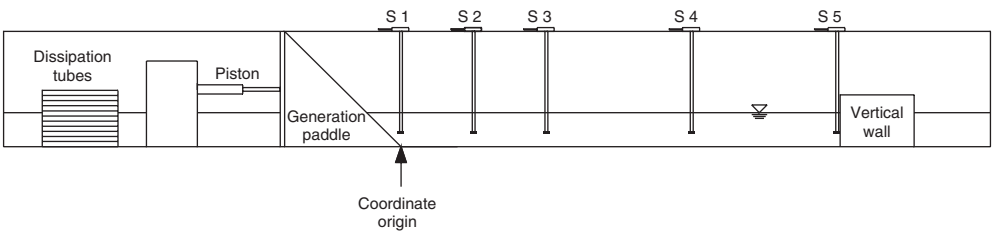

Figure 8. Wave generation and runup in a vertical wall.

Table II. Wave gauges position.

	S1	S2	S3	S4	S5	Vertical wall
45 and 60° paddles	0.00	0.50	1.00	2.00	3.00	3.01
90° paddle	Generation paddle	0.50	1.00	2.00	3.00	3.01

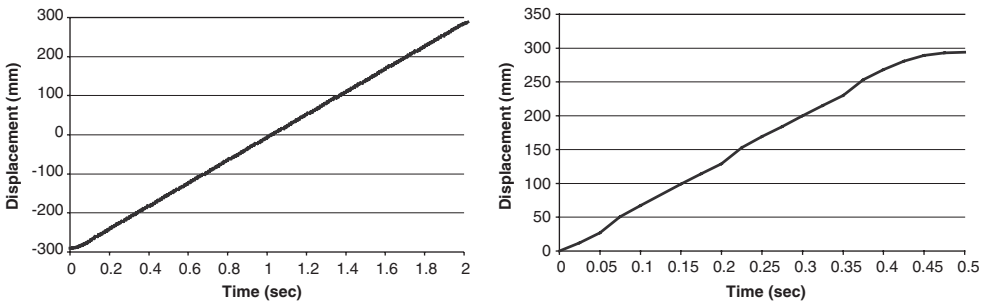

Figure 9. Generation paddle movement. Slow (left) and fast (right).

The coordinate origin is the point where the paddle intersects the flume bottom once the generation movement has finished. In the tests in which the paddle slope is 45 and 60°, the wave gauge S1 is placed in the origin of coordinates. The tests in which the paddle is vertical (90°), the gauge S1 moves with the paddle. Table II shows the position of all the gauges in each test. Coordinates are in meters and referenced to the origin of coordinates.

Three different paddle slopes were used in the tests (45, 60 and 90°) combined with two different paddle movements, referred to as 'slow movement' (SM) and 'fast movement' (FM) from now on. Both paddle movements consist of a forward movement at constant velocity (see Figure 9). The paddle stays still after this forward movement, and it does not go back to its original position. Amplitude and velocity of each motion are shown in Table III.

As can be seen in the paddle movement curves, the initial paddle acceleration, until it reaches constant velocity, and the final paddle deceleration are large enough to avoid considering them in the simulation. Thus, it will be considered that the paddle moves with constant velocity during the whole motion.

As total number of 28 tests have been analysed in this paper. To study solitary waves runup in a sloping surface four tests were conducted with water depths of 15, 20, 25 and 40 cm.

Table III. Generation paddle movement.

	Slow movement	Fast movement
Amplitude (cm)	58	29
Velocity (cm/s)	29	58

To study wave generation and reflection on a vertical wall, tests with 15, 20, 25 and 30 cm water depth were conducted. Paddles with three different slopes and two different movements were used for each water depth. These experimental results are available for further research or for other groups.

4. COMPARISON BETWEEN EXPERIMENTAL RESULTS AND NUMERICAL SIMULATIONS

4.1. Runup and breaking of a solitary wave on a sloping surface

Four different tests with water depth 15, 20, 25 and 40 cm were simulated in order to compare experimental and numerical results. Measured data are the water depth at four different gauges.

The wave is generated by a moving paddle which is situated 14 m before the sloping surface. In the numerical study only the last 6 m of the flume are simulated, as we are just interested in the study of the runup and the breaking of the solitary wave. The numerical domain consists of 3 m of flat bottom and 3 m of slanted surface. In the seaward boundary the water depth, measured by a gauge, is imposed at each time step. Each gauge register 100 measurements per second. The outward boundary condition is a reflection condition (a vertical wall is situated at the end of the flume). At the beginning of the experiment the water is at rest. The sloping surface is partially dry. In some experiments the water does not reach the end of the flume, so some cells are always dry and the vertical wall boundary condition is not used at any time step. However, the reflective wet–dry condition proposed in Section 2.3 as an internal condition is used. Figure 10 shows a comparison between the experimental and numerical results of the 40 cm water depth test. For the computations a 0.8 Courant-Friedrichs-Levy condition (CFL) is used. The grid size is 2.4 cm. The flume Manning coefficient is taken as $0.015\,\mathrm{s\,m^{-1/3}}$.

As shown in Figure 10 the code is able to predict the free water surface curvature at several time steps. The continuous line represents the numerical results while the points are for the experimental measurements registered by the four gauges. Water surface time history at the four gauges is shown in Figure 11. As is evident, numerical results are in good agreement with experimental data.

When comparing numerical and experimental data, it must be taken into account that some hypotheses which were made when developing the shallow water equations are no longer true in the tests performed. The bed slope is not small (16%). Vertical velocity and acceleration are not negligible, so the vertical pressure distribution is no longer hydrostatic. In spite of these facts, the equations are able to represent the water surface time history fairly well, although the numerical model is not able to simulate the high frequency oscillations.

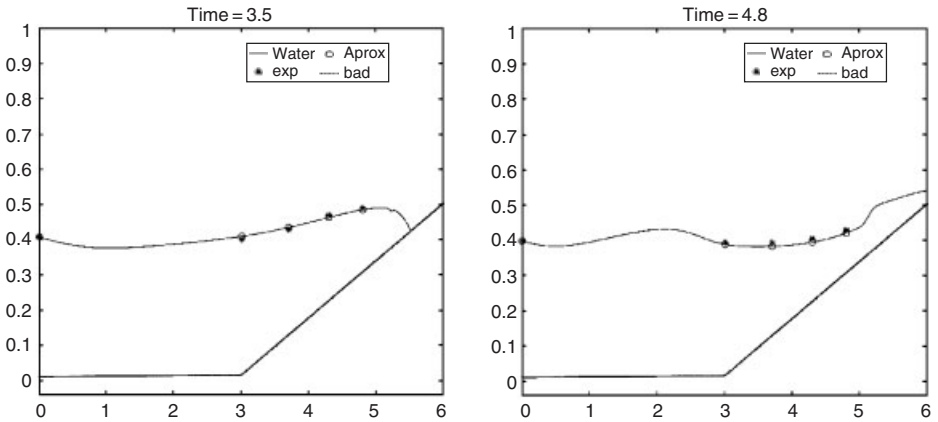

Figure 10. Breaking wave in a slanted surface. Comparison between experimental and numerical data.

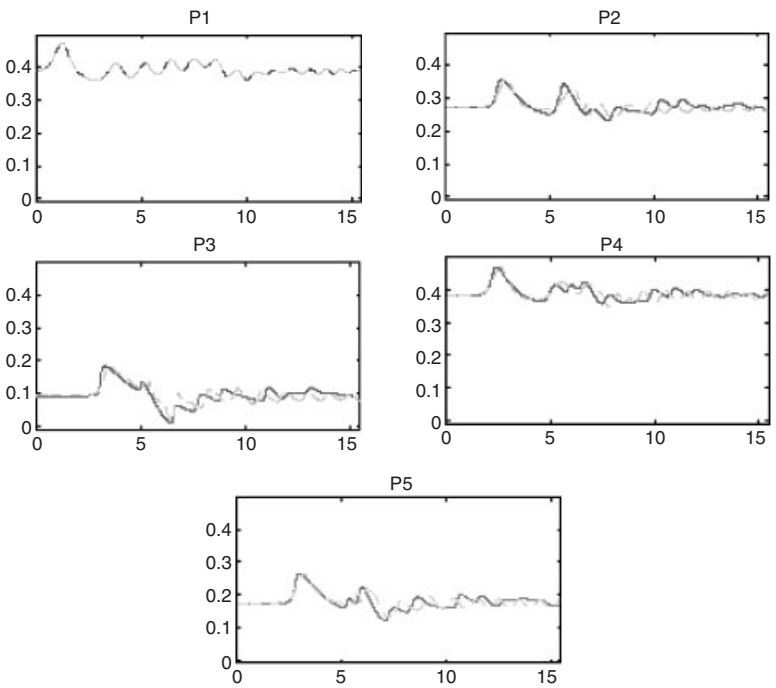

Figure 11. Comparison between experimental data (continuous) and model results (dashed).

4.2. Wave generation, runup and overtopping over a vertical wall

All laboratory tests have been numerically simulated. In the tests performed, the vertical wall was not overtopped when the still water depth is 15 or 20 cm. In the 25 and 30 cm water depth tests overtopping occurs, and it is necessary to account for it in the simulations.

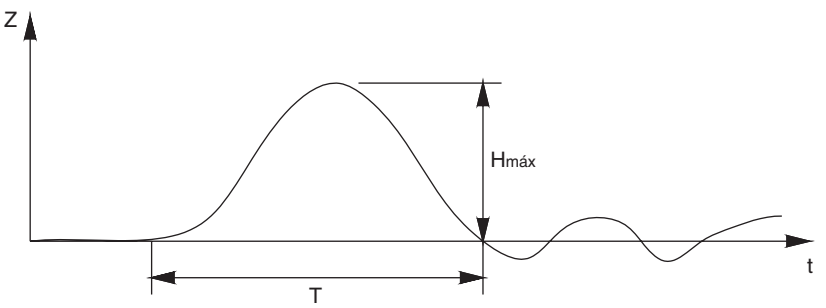

Figure 12. Wave height and period.

Table IV. Maximum water surface elevation.

	$d = 15$ cm			$d = 20$ cm			$d = 25$ cm		
	H_{exp}	$v_t = 0$	$v_t = 0.01$	H_{exp}	$v_t = 0$	$v_t = 0.01$	H_{exp}	$v_t = 0$	$v_t = 0.01$
H_{S1}	12.3	7.9	7.6	14.0	9.0	8.8	16.0	10.0	9.8
H_{S2}	11.0	7.9	7.3	12.2	9.0	8.6	13.6	10.0	9.6
H_{S3}	9.9	7.8	6.6	12.4	9.0	8.1	13.2	9.7	9.3
H_{S4}	8.2	7.0	5.2	11.1	8.5	6.7	12.0	8.7	8.1
H_{S5}	13.0	11.5	8.7	17.8	14.8	11.4	20.1	15.2	14.0

The maximum wave height and the wave period used to characterize the generated waves are shown in Figure 12. The shallow water theory is used to evaluate an approximated wave celerity as $c_{SW} = \sqrt{g(d + H_{max})}$, where g is the gravity constant, d the still water depth and H_{max} the wave height. Due to the dispersive character of the waves, which is not considered in the previous approximation, the actual celerity is smaller than the approximated celerity. The characteristic wave length L is defined as $L = cT$, where c is the wave celerity and T is the wave period.

With these parameters the adimensional parameter $2d/L$, used by Watts [2], is evaluated. The Ursell number is a ratio between non-linear and dispersive effects which is widely used to establish the dispersive character of the waves. It is defined as

$$Ur = \frac{gH_{max}T^2}{2d^2} \tag{25}$$

The bigger the Ursell number is, the non-linear effects are more important and will appear sooner.

4.2.1. Sensitivity analysis of the numerical solution to eddy viscosity. Turbulence is considered in the numerical model used. A sensitive analysis has been made in the fast movement generation tests with vertical paddle (90°). Table IV shows some results.

Although it is not conceptually true, eddy viscosity has been considered constant in space and time, so as to show the sensitivity of the numerical results to this parameter (see Figure 13).

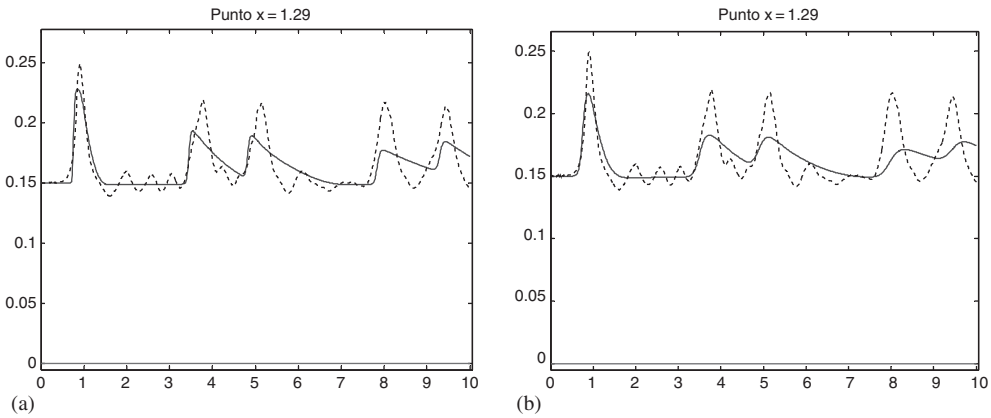

Figure 13. Sensitivity of the numerical solution to eddy viscosity: (a) 90° paddle, $d = 15$ cm, Gauge S3, $v_t = 0\,\mathrm{m}^2/\mathrm{s}$; and (b) 90° paddle, $d = 15$ cm, Gauge S3, $v_t = 0.01\,\mathrm{m}^2/\mathrm{s}$.

The greater the water depth, the greater is the turbulence importance. If a big eddy viscosity is considered, the wave height diminishes faster and the wave front profile gets smoother. If we compare the no-viscosity results with the $0.01\,\mathrm{m}^2/\mathrm{s}$ eddy viscosity results we find that a better agreement between experimental and numerical data is obtained with no-viscosity, because the turbulence generation is very small in the experimental tests. Anyway, no relevant differences were observed.

In the numerical simulations which have been made in this paper it has been considered that turbulence is not significant.

4.2.2. Fast movement. The paddle velocity in the fast movement is 58 cm/s. The movement amplitude is 29 cm. Table V shows some of the properties of the generated wave. Some parameters are obtained so as to characterize the wave generated. Experimental wave celerity C_{exp} is computed from the data registered in the S1 and S4 wave gauges as

$$C_{\mathrm{exp}} = \frac{x_4 - x_1}{t_4 - t_1} = \frac{2}{\Delta t_{1,4}} \tag{26}$$

where x_1 and x_4 are the position of wave gauges S1 and S4, t_1 and t_4 are the times at which the maximum water level is registered at gauges S1 and S4. The shallow water wave celerity is also evaluated as

$$C_{\mathrm{SW}} = \sqrt{g\left(d + \frac{H_1 + H_4}{2}\right)} \tag{27}$$

The lower the water depth the higher is the Ursell number. In all the tests the Ursell number is greater than 1, so non-lineal effects are expected. The ratio between the shallow water and the experimental wave celerities is less than 1.20 in all the tests except for 40 cm water depth with vertical paddle. This error is among the acceptable limits in water waves simulation. Kobayashi [7] considers that errors of 20% are admissible in the simulation of

Table V. Fast movement properties.

Paddle slope (deg)	Water depth d (m)	T (s)	L (m)	H_{max} (m)	$2d/L$	Ur	C_{exp} (m/s)	C_{sw} (m/s)	C_{sw}/C_{exp}
45	0.15	0.74	1.15	0.095	0.26	11.33	1.54	1.55	1.01
45	0.20	0.82	1.41	0.102	0.28	8.40	1.65	1.71	1.03
45	0.25	0.89	1.66	0.107	0.30	6.64	1.71	1.85	1.08
45	0.30	0.97	1.95	0.113	0.31	5.79	1.77	1.99	1.12
45	0.40	0.99	2.22	0.114	0.36	3.42	1.87	2.22	1.19
60	0.15	0.59	0.93	0.105	0.32	7.96	1.60	1.58	0.99
60	0.20	0.65	1.15	0.119	0.35	6.16	1.67	1.74	1.05
60	0.25	0.72	1.38	0.127	0.36	5.16	1.74	1.89	1.09
60	0.30	0.74	1.53	0.135	0.39	4.02	1.83	2.03	1.10
60	0.40	0.81	1.87	0.143	0.43	2.87	1.92	2.26	1.18
90	0.15	0.59	0.97	0.123	0.31	9.32	1.61	1.57	0.98
90	0.20	0.59	1.08	0.140	0.37	5.97	1.69	1.79	1.05
90	0.25	0.60	1.20	0.159	0.42	4.49	1.72	1.95	1.13
90	0.30	0.56	1.20	0.172	0.50	2.94	1.80	2.09	1.16
90	0.40	0.62	1.50	0.196	0.53	2.31	1.92	2.34	1.22

solitary waves. In most tests C_{exp} is smaller than C_{SW}. The difference between both is greater at bigger water depths. This difference is because there is no consideration of dispersive effects in CSW. Figure 14 shows the generation of small crests as the wave progresses. These small crests are due to the vertical velocities and accelerations of the water particles that are not considered by the shallow water models. However, the model predicts fairly well the mean water surface level, as it can be observed in Figure 14.

As it is shown in Figure 14, experimental data oscillate around the numerical data. As it has been mentioned before, this is because there is no consideration of vertical velocity in the shallow water equations. A measurement of the error of the numerical simulation is defined in order to verify that there is no trend in the experimental data. This error is defined considering the total area between the experimental and numerical curves. The error is zero if the numerical data is the mean value of the experimental data.

$$\text{error} = \sum_{i=1}^{n} \frac{(h_i^{\text{exp}} - h_i^{\text{num}})\Delta t}{t_{\max} H_{\max}} \tag{28}$$

where n is the number of experimental data, h_i^{exp} are the experimental data, h_i^{num} are the numerical data, Δt is the time step between two consecutive datum, $t_{\max}$ is the total time of computation and $H_{\max}$ the maximum wave height as defined in Figure 12. Table VI shows the error at each measurement point.

As a consequence of the dispersive effects, the agreement between the prediction of the water surface and the experimental data varies in time. However, a good general approach can be observed, as shown in Figure 15.

If we represent the error versus time, it can be observed that the error oscillates around its mean value (see Figure 16). This means that the error in the numerical simulation is mainly due to the high frequency water level oscillations, which cannot be simulated by the numerical model. However, for big time steps the mean error is not zero.

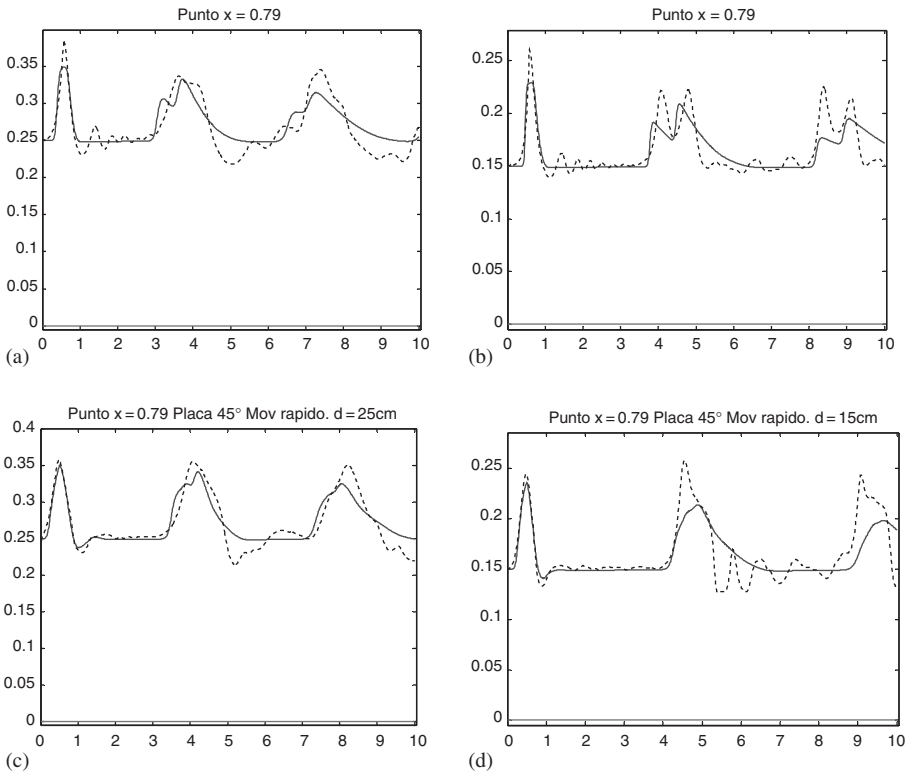

Figure 14. Fast movement. Comparison between experimental and numerical data: (a) 90° paddle, $d = 25$ cm, Gauge S2, 200 nodes; (b) 90° paddle, $d = 15$ cm, Gauge S2, 200 nodes; (c) 45° paddle, $d = 25$ cm, Gauge S1, 100 nodes; and (d) 45° paddle, $d = 15$ cm, Gauge S1, 100 nodes.

Table VI. Error in the fast movement.

Paddle slope (deg)	Water depth d (m)	Gauge 1	Gauge 2	Gauge 3	Gauge 4	Gauge 5
45	0.15	0.0249	0.0474	0.0069	0.0267	0.0053
45	0.20	0.0112	0.0013	0.0147	0.0213	0.0071
45	0.25	0.1215	0.0178	0.0308	0.0271	0.0218
45	0.30	0.1416	0.0051	0.0212	0.0549	0.0062
60	0.15	0.0514	0.0419	0.0295	0.0124	0.0229
60	0.20	0.0773	0.0597	0.0504	0.0588	0.0689
60	0.25	0.0370	0.0043	0.0213	0.0236	0.0015
60	0.30	0.0244	0.0096	0.0370	0.0252	0.0002
90	0.15	0.0122	0.0046	0.0030	0.0001	0.0050
90	0.20	0.0046	0.0229	0.0207	0.0136	0.0022
90	0.25	0.0113	0.0239	0.0252	0.0189	0.0014
90	0.30	0.0162	0.0297	0.0337	0.0227	0.0015

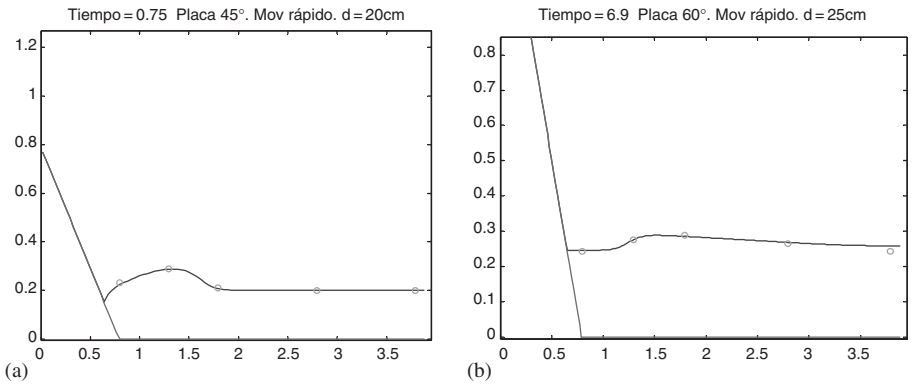

Figure 15. Fast movement. Free water surface level. Model prediction (Continuous line). Experimental data (points): (a) 45° paddle, $d = 20$ cm, time step $= 0.75$ s, 100 nodes; and (b) 60° paddle, $d = 25$ cm, time step $= 6.9$ s, 200 nodes.

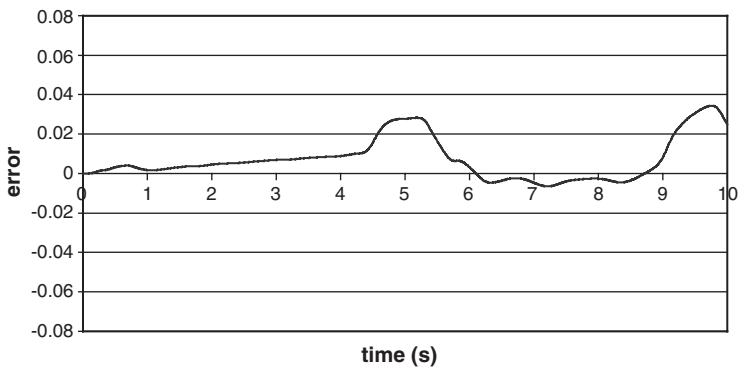

Figure 16. Fast movement. Error vs time at wave gauge S1, 45° paddle and water depth 15 cm.

4.2.3. Slow movement. The paddle velocity in the slow movement is 29 cm/s. The movement amplitude is 58 cm. The properties of the generated wave are shown in Table VII.

As in the fast movement, the ratio between theoretical and experimental wave celerity is always less than 1.20 (see Table VII). The Ursell number is much higher than in the fast movement. This is because the duration of the slow movement (2 s) is higher than the duration of the fast movement (0.5 s) so the wave period is higher in the first case. As shown in Figure 17, when generating the wave with this movement, the water surface level oscillates around an equilibrium level. The numerical method predicts the equilibrium level (see Figure 18), but, once again, it is not able to predict the high frequency oscillations. The bigger the generation paddle slope is, the bigger are these oscillations.

For this kind of movement, the error defined by (28) at each measurement point is shown in Table VIII (see Figure 19).

Table VII. Slow movement properties.

Paddle slope (deg)	Water depth d (m)	T (s)	L (m)	H_{max} (m)	$2d/L$	N° Ursell	C_{exp} (m/s)	C_{sw} (m/s)	C_{sw}/C_{exp}
45	0.15	2.32	3.25	0.050	0.09	58.61	1.36	1.41	1.04
45	0.20	2.39	3.77	0.054	0.11	37.79	1.50	1.59	1.06
45	0.25	2.47	4.31	0.060	0.12	28.70	1.67	1.75	1.05
45	0.30	2.52	4.76	0.064	0.13	22.13	1.74	1.90	1.09
45	0.40	2.67	5.76	0.075	0.14	16.37	2.11	2.16	1.03
60	0.15	2.2	3.10	0.053	0.10	55.86	1.35	1.42	1.05
60	0.20	2.23	3.55	0.058	0.11	35.33	1.49	1.59	1.07
60	0.25	2.27	3.99	0.065	0.13	26.26	1.63	1.76	1.08
60	0.30	2.3	4.37	0.068	0.14	19.58	1.69	1.90	1.12
60	0.40	2.33	5.04	0.077	0.16	12.80	1.85	2.17	1.17
90	0.15	2.14	3.01	0.052	0.10	51.86	1.39	1.42	1.02
90	0.20	2.14	3.41	0.059	0.12	33.10	1.49	1.60	1.08
90	0.25	2.14	3.77	0.067	0.13	24.06	1.60	1.77	1.11
90	0.30	2.14	4.09	0.073	0.15	18.20	1.72	1.91	1.11
90	0.40	2.15	4.68	0.083	0.17	11.75	1.88	2.18	1.16

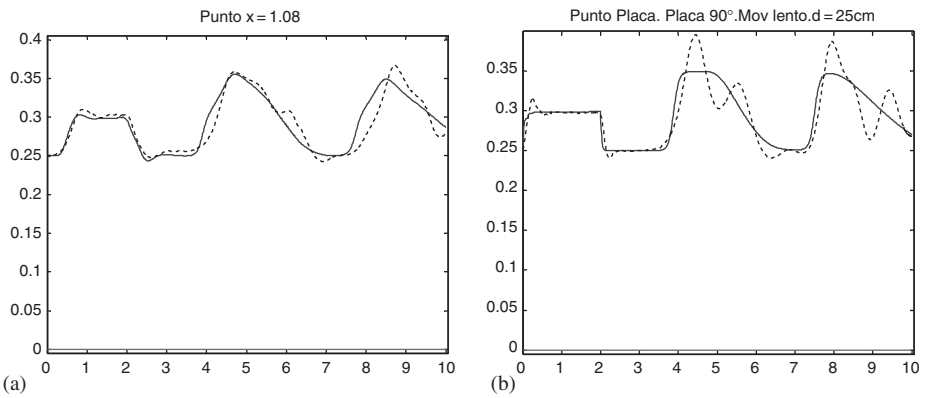

Figure 17. Slow movement. Water surface elevation at gauge S1. Comparison between experimental and numerical data: (a) 45° paddle, $d = 25$ cm, Gauge S1, 100 nodes; and (b) 90° paddle, $d = 25$ cm, Gauge S1, 100 nodes.

Figure 20 shows the ratio maximum wave height–equilibrium height. This ratio is nearly constant when the generation paddle slope is 90°, but it diminishes with the still water depth when the paddle slope is 60 or 45° (see Tables IX and X).

Experimental and numerical equilibrium heights agree very well. The approximation proposed in Section 2.4.1 ($H_{2.4.1}$) also agrees with experimental data.

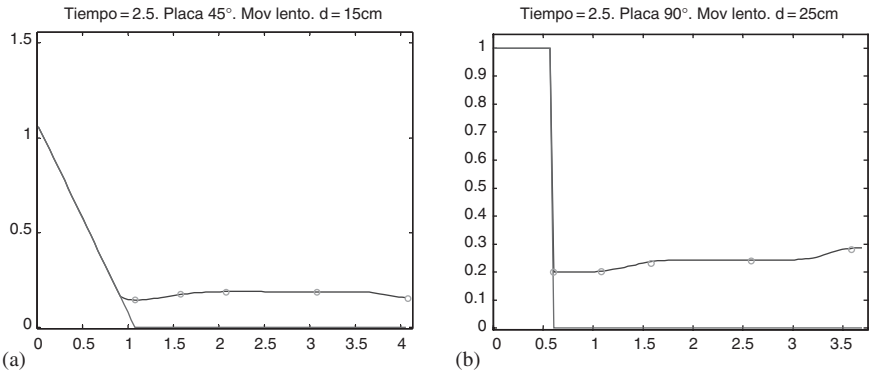

Figure 18. Slow movement. Free water surface level. Model prediction (continuous line) and experimental data (points): (a) 45° paddle, $d = 15$ cm, Time step $= 2.5$ s, 100 nodes; and (b) 90° paddle, $d = 20$ cm, time step $= 2.5$ s, 100 nodes.

Table VIII. Error in the slow movement.

Paddle slope (deg)	Water depth d (m)	Gauge 1	Gauge 2	Gauge 3	Gauge 4	Gauge 5
45	0.15	0.0200	0.0172	0.0520	0.0352	0.0320
45	0.20	0.0030	0.0352	0.0700	0.0407	0.0180
45	0.25	0.0442	0.0340	0.0783	0.0910	0.0583
45	0.30	0.0250	0.1250	0.0859	0.1844	0.0906
60	0.15	0.1887	0.0528	0.0774	0.0642	0.0472
60	0.20	0.2103	0.0103	0.0336	0.0448	0.0167
60	0.25	0.0200	0.0277	0.0585	0.0585	0.0785
60	0.30	0.0053	0.0294	0.0735	0.0971	0.0721
90	0.15	0.0360	0.0158	0.0179	0.0181	0.0150
90	0.20	0.0251	0.0214	0.0129	0.0415	0.0203
90	0.25	0.0179	0.0134	0.0403	0.0373	0.0164
90	0.30	0.0233	0.0192	0.0411	0.0616	0.0411

5. CONCLUSIONS

Numerical models based on the shallow water equations are widely used in the simulation of the propagation and breaking of long water waves. In this paper, a finite volume numerical model which has been verified in several previous studies is used to solve the one-dimensional shallow water equations and predict the generation, propagation and reflection of solitary waves. Numerical results have been compared with experimental laboratory tests made specifically for this investigation.

A new wet–dry condition is proposed to compute wave runup and reflection. The performance of this new condition is evaluated in a first series of tests in which the runup and breaking of a solitary wave to a slanted surface is studied. Later on, this condition is used in a second series of tests to compute wave reflection in a vertical wall. The wet–dry condition is also used to account for a vertical overtopping wall. In both simulations good results are achieved.

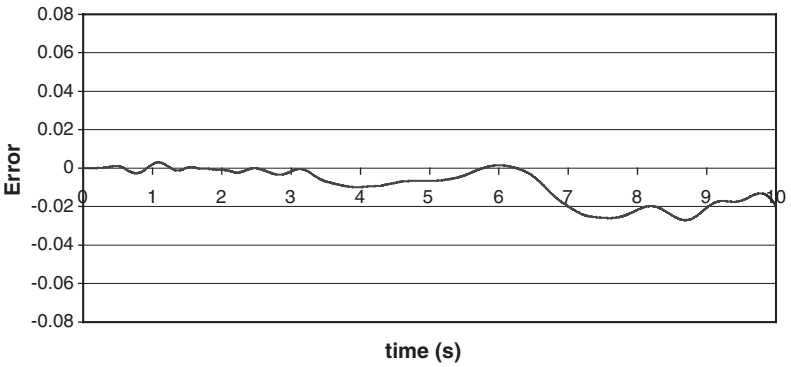

Figure 19. Slow movement. Error vs time at wave gauge S2, 90° paddle and water depth 30 cm.

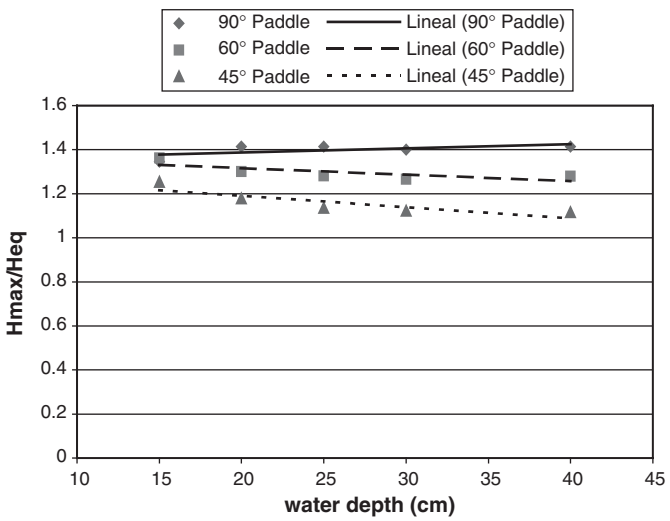

Figure 20. Maximum wave height–equilibrium height ratio.

Table IX. Lineal regression $y = H_{\max}/H_{\text{eq}}$, $x =$ water depth.

90° Paddle	$y = 0.0019x + 1.3491$
60° Paddle	$y = -0.0029x + 1.3746$
45° Paddle	$y = -0.0051x + 1.2929$

To simulate the generation of a water wave by the movement of a slanted surface, two different schemes, depending on the slope of the surface, are proposed. When the wave is generated by a vertical wall, a specific boundary condition for this particular case is used. Generation of waves by a slanted surface is achieved by a bed movement, making use of the wet–dry condition. The performance of both schemes is acceptable. Differences observed

Table X. Equilibrium wave height.

Paddle slope (deg)	Water depth d (cm)	H_{exp} (cm)	H_{num} (cm)	$H_{2.4.1.}$ (cm)
45	15	3.95	3.90	—
45	20	4.56	4.40	—
45	25	5.20	5.00	—
45	30	5.62	5.20	—
45	40	6.65	6.20	—
60	15	3.85	3.90	—
60	20	4.42	4.40	—
60	25	5.01	5.00	—
60	30	5.35	5.40	—
60	40	6.10	6.15	—
90	15	3.85	3.90	3.78
90	20	4.20	4.30	4.34
90	25	4.75	4.90	4.83
90	30	5.20	5.30	5.27
90	40	5.90	6.10	6.06

between experimental and numerical results are due to the nature of the shallow water equations and have nothing to do with the wave generation boundary conditions. The main problem is the existence of vertical velocities and accelerations which invalidate the hydrostatic pressure hypothesis made in the shallow water model. The greater the slope of the slanted paddle, the greater are the vertical velocities and accelerations.

Two limitations in the application of the shallow water equations have been found. It has been observed that the numerical model predicts the wave breaking before it occurs in the experimental tests. The second limitation has to do with the maximum wave height. The model is able to predict the mean movement of the water surface, but it is not able to simulate the high frequency oscillations around this mean level. This is an important limitation to be considered, because the model underpredicts the maximum water depth, which is an important parameter in the design of dams, bridges or similar civil structures.

REFERENCES

1. Wiegel RL. Laboratory studies of gravity waves generated by the movement of a submerged body. *Transaction of American Geophysical Union* 1995; **36**:759–774.
2. Watts P. Tsunami features of solid block underwater landslides. *Journal of Waterway, Port, Coastal, and Ocean Engineering* 2000; **126**:144–152.
3. Lin P, Chang K, Liu PLF. Runup and rundown of solitary waves on sloping beaches. *Journal of Waterway, Port, Coastal, and Ocean Engineering* 1999; **125**:247–255.
4. Harten A, Lax P, van Leer A. On upstream differencing and Godunov-type schemes for hyperbolic conservation laws. *SIAM Review* 1983; **25**:35–61.
5. Vázquez-Cendón ME. Improved treatment of source terms in upwind schemes for the shallow water equations in channels with irregular geometry. *Journal of Computational Physics* 1999; **148**:497–525.
6. Brufau P, Vázquez-Cendón ME, García-Navarro P. A numerical model for the flooding and drying of irregular domains. *International Journal for Numerical Methods in Fluids* 2002; **39**:247–275.
7. Kobayashi N, Tega Y. Numerical prediction of solitary wave runup on vertical walls by finite-amplitude shallow-water model. In *Long-Wave Runup Models*, Yeh H, Liu P, Sinolakis C (eds). World Scientific: Singapore, 1996; 88–115.

